Design of Functionalized Nanoparticles for the Applications in Nanobiotechnology

*Kazuo Tanaka and Yoshiki Chujo**

Department of Polymer Chemistry, Graduate School of Engineering, Kyoto University,

Katsura, Nishikyo-ku, Kyoto 615-8510, Japan

E-mail: chujo@chujo.synchem.kyoto-u.ac.jp

Phone: +81-75-383-2604

Fax: +81-75-383-2605

Keywords:

Nanoparticle, Superparamagnetic iron oxide, Silica, Gold, Bioprobe

Abstract:

We review the design and synthesis of functionalized nanoparticles for the application in nanobiotechnology. Initially, the modification of the superparamagnetic iron oxide (SPIO) for contrast agents is described. The series of biomolecule-responsive contrast agents are introduced. Next, silica nanoparticle-based probes in ^{19}F NMR are explained. By employing the silica nanoparticles as a signal quencher for NMR signals, the quantitative analysis of the enzymatic activities was accomplished. The design concepts and the results are explained. We also mention the regulation of the cluster formation of gold nanoparticles. Significant changes in optical properties before and after the assembly are presented. Finally, the typical synthetic procedures are also described in the latter part.

Introduction:

Nanoparticles have attracted attention as a scaffold to obtain smart biomaterials because of several advantages: Firstly, the biodistribution of the nanoparticles can be modulated by changing the size of the particles. For example, as we presented in this paper, silica-based nanoparticles are versatile materials for designing functional bioprobes and the vesicles for drug delivery because of their high stability and the flexibility in the modification. Because various size and surface-modified silica nanoparticles can be readily prepared, we can deliver drugs or other bioactive materials to the target sites by loading onto the nanoparticles with the size effects on the distribution. In particular, nanoparticles in the range of 20 nm to 400 nm in diameter show tumor-selective integration known as the enhanced permeability and retention (EPR) effect.[1–7] Therefore, the site-specific delivery can be realized based on the preprogrammed designs. Secondly, the local concentrations of the loaded drugs can be readily enhanced. In the case of the drugs with small molecular weights, the drug concentrations could be lowered by the diffusion. On the other hand, since the nanoparticles have better retention ability than those of small molecules, it is relatively easy to keep the local concentration to receive enough drug efficiency. In addition, if the nanoparticle can slowly release the loaded drugs, the sustained release system can be readily realized. Thirdly, the diverse properties can be obtained not only originated from the intrinsic properties of the component elements or the surface modification but also from the nano-sized effects of the particles. For example, the nanoparticles composed of ferromagnetic iron oxide show similar behaviors, called superparamagnetism, to the paramagnetic materials such as no hysteresis and no residual magnetization.[8,9] These materials are used as a conventional contrast agent in magnetic resonance imaging

(MRI). In the case of gold nanoparticles, the absorption bands in the visible region can be observed. Various kinds of biosensors have been invented based on the gold nanoparticles. The nanoparticles composed of semiconductor materials called as quantum dots show various emission colors depended on their diameters.[10–13] Based on these characteristics derived from the size effects, unique optical bioprobes have been developed. In this review, we survey the functionalized nanoparticles for the application in nanobiotechnology. Our recent studies on the development of bioprobes or bio-related materials with the series of nanoparticles composed of iron oxide, silica and gold are mainly introduced. The typical synthetic procedures are also described in the latter part.

Superparamagnetic iron oxide

MR sensors for biomolecules

Initially, we present the superparamagnetic iron oxide (SPIO)-based contrast agents in magnetic resonance imaging (MRI). MRI is one of the powerful and conventional diagnostic tools in modern clinical medicine for the 3D visualization inside vital bodies with high resolution. In particular, by using contrast agents, sensitivity and specificity in the detection can be extensively improved. The SPIOs are magnetite crystals with several nanometer sizes.[8,9] In the magnetic fields, SPIOs can accelerate the proton transverse relaxation of water tissue in aqueous media and consequently provide hypointense (dark) contrast in magnetic resonance images on T_2 and T_2*-weighted sequences. SPIO-based contrast agents are already commercially available and used at the clinical stages. Moreover, various techniques using SPIOs such as the cell labeling[14–18], biosensors[19–22], and in vivo imaging[23–26] with MRI have been developed.

Thus, the SPIO-based contrast agents can be a suitable platform for designing the advanced imaging probes. In this part, the regulations of the magnetism by modulating the aggregation/dispersion of the SPIO particles and their applications for biosensors in MRI are presented.

By the formation of assembly, the magnetism of SPIOs can be enhanced, resulting in much darker contrasts in the MR images. Based on these phenomena, various kinds of biosensors have been prepared with the modified SPIOs.[19–22] We also have aimed to develop the biomolecule-responsive SPIOs. Particularly, the surface modified-SPIOs were prepared for detecting the bio-significant molecules and environmental factors such as protein, gene, and pH.

We designed the surface modification of SPIOs for realizing the target-responsive cluster formation with the variety of biomolecules.[27] Figure 1 outlines the system of the modified SPIOs. We initially synthesized the biotin-presenting SPIOs to form the cluster in the presence of an avidin protein. As shown in Figure 2a, the precipitation was confirmed by the naked eyes immediately after adding avidin to the solution containing the biotin-presenting SPIOs. From the DLS measurements, the increase of the observed hydrodynamic radius (r_H) of the biotin-presenting SPIOs (19.5 ± 5.2 nm) to be 51.2 ± 22.4 nm was monitored by adding the 2000-times diluted avidin solution. Consequently, we showed this system can represent the highly-sensitive protein sensor by the naked eyes with the minimum detection limit of 10 fmol of avidin with the biotin-presenting SPIOs.

(Figures 1 and 2)

The hemin-presenting SPIOs were prepared and added to the aptamer DNA which can selectively recognize hemin with high affinity[28] in the buffer solution (Figure 2b). The cluster of the SPIOs was obtained only from the sample containing both the aptamer DNA and the target sequence after 15 min standing. On the other hand, slight precipitation was obtained from the negative controls. These data indicate that the cluster of the SPIOs can be obtained via the hemin-aptamer interaction. By replacing hemin to other small molecules which are applicable as a target for the aptamer, diverse detection systems can be prepared.

As compared to the dispersion states, the SPIO clusters can much efficiently enhance the transverse relaxation of water tissues. Therefore, a darker contrast can be obtained in the T_2-weighted MR image. To present the MR sensor for gene expression, we investigated the cluster formation of the DNA-presenting SPIOs in the presence of the complementary strand.[27] Figure 3 shows the T_2-weighted MR image of the samples containing the DNA-presenting SPIOs at 7 T at 25 °C. We also evaluated the T_2 relaxation times of each solution. The significant decreases of the T_2 values appeared from the sample containing the target DNA (40 fmol). The MR image showed the darker effect at the modified SPIOs-containing samples, corresponding to the decreases of the T_2 values. These data mean that the sequence-specific NMR probe can be obtained. In addition, the sensitivity can be improved approximately 10-fold higher than that of previous system reported as a highly-sensitive MRI sensor.[29]

(Figure 3)

The SPIOs which can form the aggregation under slightly acidic condition are promised to be a labeling agent for tumor tissues because it is known that the pH values of the tumor tissues are from 0.4 to 1.0 units lower than those of the normal tissues.[30–33] Next, we aimed to establish the regulation of aggregation/dispersion of the SPIOs by the pH alteration under slight acidic condition in the narrow region. According to the previous works, the pH-responsiveness of the metal nanoparticles showed good agreements with the dissociation constants of the acid groups of the surfactants.[34,35] For instance, the carboxylic acid-presenting gold particles can form the aggregation below pH 3.8.[34] In the case of the phosphonic acid-presenting gold particles, the cluster formation can be observed below pH 5.5.[35] Arsonic acid has higher acid dissociation constant (pK_{a1} = 4.5) than those of carboxylic acid (pK_a = 4.0) or phosphoric acid (pK_{a1} = 2.0).[36] Hence, we focused on arsonic acid derivatives as new series of the surface modifications for providing the particles with the ability to change the dispersion state under mild acidic conditions.

Arsonic acid-presenting SPIOs were prepared, and the pH-responsiveness was examined (Figure 4).[37] We synthesized arsonoacetic acid as the stabilizer for the SPIOs. The desired SPIO particles were prepared by a ligand exchange from the undecanoic acid ligand. The resulting SPIOs showed good dispersibility only in water. From the FT–IR spectra, it was shown that arsonoacetic acid should largely coordinate to the particles at the carboxylic unit, but not at the arsonic acid unit as shown in Figure 4. This means that the arsonic acid groups should be presenting from the surfaces of the

SPIOs. Based on these characterization data, we concluded that the desired arsonic acid-presenting SPIOs can be obtained.

(Figure 4)

To examine the pH-responsiveness of the arsonic acid-presenting SPIOs, the r_H values were monitored with DLS measurements at variable pH (Figure 5a). The SPIOs were well-dispersed at pH 9. In the pH range from 7 to 9, the r_H values observed from the dispersions were slightly changed. In contrast, the r_H value immediately increased at pH = 6.1 with the formation of the precipitation. Subsequently, the r_H values reached a plateau below pH 6. These behaviors mean that the arsonic acid-presenting SPIOs can form the clusters with borderline at pH 6.1. Moreover, the aggregation/dispersion states of the SPIOs can be switched through several pH changes (Figure 5b). Furthermore, the darker contrasts were obtained from the clusters of the SPIOs. It should be mentioned that precipitation or color changes were hardly observed during the pH titration. Average diameters of the particles subtly changed from the pristine dispersion. These data represent the important issue that the arsonic acid unit can be stably immobilized on the surface of the SPIOs in this pH region. In other words, the arsonic acid species should be less released from the surface. These results clearly indicate that the arsonic acid-presenting SPIOs should be a pH-responsive probe for slight acidic regions.

(Figure 5)

Tumor-specific prodrugs using arsonic acid-presenting SPIOs

The further functions of the arsonic acid-presenting SPIOs in the cells were obtained.[38] As we mentioned, if it is possible to precisely recognize the differences of the environmental factors between tumor and normal cells, we can obtain tumor-selective probes. Furthermore, if these discrimination ability between tumor and normal cells can be used as a trigger for activating prodrugs which must undergo chemical conversion by metabolic processes before becoming an active pharmacological agent, we can expect to receive highly-specific anticancer drugs, leading to the suppression of the administration amounts and undesired adverse effects.[39,40] Reductive environments in the tumor cells were one of significant differences in the active tumor regions.[41–43] Intracellular reductive environments are mainly controlled by modulating the amount of thiol groups in the reduced glutathione (GSH).[44–46] Therefore, the thiol-responsive functional groups or molecules can be a candidate for the designs of the reduction-responsive prodrugs. Indeed, reductive environment-responsive prodrugs were developed not only for the imaging of cancer regions but also for anticancer drugs.[39] Based on these backgrounds, we focused on the As(V)–C bond as a reduction-responsive unit for the tumor-specific prodrug. In the presence of the reducing agent such as GSH, the transformation from As(V) to As(III) proceeds with the bond cleavage of As–C, resulting in the generation of highly-toxic arsenic species (Figure 6).[47,48] Since the concentrations of GSH in tumor cells are higher than those in normal cells, the transformation from As(V) to As(III) could be enhanced. Consequently, the tumor-selective cell death would be induced.[49,50] To confirm these idea, the cytotoxicity of the arsonic acid-presenting SPIOs was investigated.

(Figure 6)

The influence on the cell viability was investigated in the presence of the modified nanoparticles, arsenic trioxide (As_2O_3) as a positive control, and the water-dispersive naked nanoparticles as a negative control with various concentrations.[38] Figure 7 shows the cell viabilities after 72 h incubation with the samples. While the strong toxicity was confirmed from As_2O_3 to the tumor cells, the naked nanoparticles slightly affected the cell viability through the entire concentration range. Significantly, the viability of the cancer cell line was also maintained in the presence of the arsonic acid-presenting SPIOs. These data clearly indicate that the arsonic acid-presenting SPIOs should show cancer cell-selective cytotoxicity.

(Figure 7)

Cluster formation of SPIOs by employing ionic liquid chemistry

An ionic liquid (IL) is a nonvolatile salt with a melting temperature below 100 °C. By modifying the surface of the metal nanoparticles with the IL molecules, the versatile properties similarly observed in the pure ILs can be obtained.[51–54] For instance, counter anion exchange with the ion pair can readily and quantitatively proceed under mild conditions, leading to the drastic property changes.[53] Therefore, this alteration can be used as a conventional platform for realizing stimuli-responsiveness. In the previous reports, the influence on aggregation/dispersion states of the metal nanoparticles was investigated by adding ionic salts which are promised to be the counter anion.[54] Accordingly, the dispersion states can be changed via significant changes of the hydrophobicity depended on the counter anions. These changes proceeded rapidly under

mild conditions with other kinds of metal nanoparticles. We aimed to apply these changes on the regulation of the aggregation/dispersion states of SPIOs.

We synthesized three types of the phosphonium-presenting SPIOs as shown in Figure 8.[55] To inhibit undesired interaction between the ionic species and the surface of the nanoparticles and reinforce the stability of the phosphonium cation, we introduced the silica layer at the surface of the SPIO. **NP1** and **NP2** are covered with the bilayer with or without the silica layer at the surface between the SPIO core and the inside layer, respectively. The phosphonium cation is tethered to the SPIO core via the silica layer on **NP3**.

(Figure 8)

The dispersion states of the phosphonium-presenting SPIOs were monitored during anion exchange.[55] To the aqueous dispersions of phosphonium bromide-presenting SPIOs, **NP1** and **NP2**, NaCl and potassium bis(trifluoromethanesulfonyl)amide (KTFSA) were added, respectively (Figure 9). By adding NaCl, all SPIOs maintained the dispersion states. In contrast, the significant aggregation of **NP2** was immediately observed after adding KTFSA. Similar result was obtained from **NP3**. These data can be explained by the structures of the surface modification. The phosphonium cations are weakly anchored via bilayers at the surface of **NP1**. The desorption of the phosphonium cations could occur after formation of the strong hydrophobic TFSI salts. Thereby, the hydrophilicity of the surface should be maintained. On the other hand, the strong hydrophobic TFSI salts should be stayed at the surface of **NP2** and **NP3** via the robust

immobilization of the phosphonium cations. Thereby, the aggregation should be formed via the hydrophobic interactions. These results present that the dispersion/aggregation behavior of nanoparticles should be modulated by modification manners.

(Figure 9)

Catch and release of DNA with SPIOs

The biotechnological applications of anion exchange for the DNA separation are demonstrated.[56] The catch and release technique with DNA was established via anion exchange with imidazolium-presenting nanoparticles (Figure 10). As a background, isolation of nucleic acids is a fundamental and essential technique in biotechnology.[57] The target sequence must be extracted from biological samples without damage during operations in the sequencing and the preparing of DNA library. Therefore, it is favorable to perform for the extraction of nucleic acids under mild conditions. SPIOs have been conventionally used for the bio-related materials involving for nucleic acids collection.[51] Based on attractive forces with a magnet, the target molecules and sequences can be readily collected. The development of the release procedure under mild condition is beneficial to collect the target molecules without damage or denaturation.

(Figure 10)

We prepared the water-dispersive imidazolium-presenting SPIOs (Im-SPIOs), and the adsorption of DNA onto Im-SPIOs was investigated.[56] To the solutions of the plasmid

DNA in the buffer, the dispersion of the SPIOs was added. After vortex, Im-SPIOs were collected with a magnet, and the supernatants were transferred to new tubes. After centrifugation, the samples were applied on the agarose gel, and the residual amounts of DNA were evaluated. Accordingly, by adding Im-SPIOs, the concentration of the plasmid DNA was obviously reduced. These data indicate that Im-SPIOs can capture DNA. The release of DNA via anion exchange was carried out with Im-SPIOs. Similarly as the adsorption experiments, the plasmid DNA was mixed with the modified nanoparticles. After washing, the KTFSA solution was added for anion exchange from Cl^- to $TFSA^-$. The supernatant was collected and applied on the gel after centrifugation. The band was observed from the sample with the KTFSA treatment (Figure 11). Moreover, these catch and release system can be worked in the fetal bovine serum. These data clearly indicate that catch and release of DNA can be controlled with Im-SPIOs by altering the counter anion. It should be mentioned that the heating or drastic pH changes are not necessary all through the operations.

(Figure 11)

Improvement of sensitivity of MR contrast agents

By introducing the silica layer at the surface of SPIOs, the improvement of the stability at the dispersion states can be expected. Undesired aggregation or non-specific adsorption with biomolecules can be suppressed. In addition, the further modification with functional molecules is applicable as presented above. The size, shape, and the surface modification which dominate the characteristics, distribution, and toxicity of the particles can be readily tuned.[52] We have reported the preparation method of the MRI

contrast agents based on the silica-coated core/shell type SPIO particles which can show good biocompatibility in the mice.[51] However, the decrease of the sensitivity in MRI was inevitable by the silica coating on the surfaces. To compensate the loss of the sensitivity, we challenged to establish the new concept for the development of highly-sensitive SPIO-based contrast agents. As we mentioned in the former part, the magnetism of SPIOs can be enhanced by the formation of assembly.[27] As a result, much darker contrasts can be obtained in the MR images. Based on this phenomenon, we designed the multi SPIOs-involving silica-coated core/shell type particles.

The preparation of the desired particles is composed of two steps[58]: the separation and the etching of the shell (Figure 12). Initially, the silica-coated SPIO particles were prepared via a reverse-micelle sol-gel technique.[51] We executed the centrifugal separation in the isopycnic density media.[59] Under the optimized centrifugal condition, the silica-coated core/shell type particles including multiple SPIOs were obtained in good yields. The etching treatment was performed under strong alkaline conditions to melt the silica layer on the particles. After the incubation, the surface of the particles was modified with imidazolium, and well-dispersed suspension can be prepared. The iron content in the particles was significantly improved by the etching process.

(Figure 12)

The T_2-weighted MR image of the samples containing the SPIO particles is shown in Figure 13.[58] We determined the detection limits of each particle toward contrast enhancement. The sample without both treatments showed less dark contrast. On the

other hand, the samples after the centrifugation step showed the enhancement of the transverse relaxation. In particular, the multi-core SPIO particles after etching gave much clearer contrast even at 3.5 μg/mL of iron concentration. These results suggest that the sensitivity to create negative contrast can be improved at least 7-times larger than that of the sample before treatments. It was found that the relaxation ability was improved approximately 3-fold higher than that of previous system reported as a highly-sensitive MRI sensor.[29,60]

(Figure 13)

Silica nanoparticles

Design of ^{19}F NMR probes for quantitative detection of enzymatic activity

Silica nanoparticles are versatile scaffolds for constructing functional bio-related materials. From the sol–gel reactions firstly reported by Stöber *et al.*[61], various sized particles (10^{-8} m to 10^{-6} m) can be readily prepared with small size-distribution in good yields only by modulating the reaction conditions. In addition, various modifications and the loading of the functional molecules such as drugs or dyes are acceptable at the surface of nanoparticles. Particularly, because of transparency of silica, a wide variety of emissive particles have been manufactured with silica nanoparticles.[62] In this part, we introduce the silica nanoparticle-based bioprobes. In particular, the design concepts and the results on the quantitative measurements of bioreactions with a ^{19}F NMR spectroscopy are described here.

By using the fluorinated compounds as a contrast agent, the highly-resolved images

at the deep spot inside vital bodies with the high signal to noise ratio can be obtained in ^{19}F MRI because of less existence ratio of endogenous fluorine atom.[63–65] We focused on these advantages and aimed to develop the ^{19}F MR probes for monitoring the biological reactions at the molecular levels. In this part, the series of our ^{19}F MR probes based on the modified silica nanoparticles are introduced. In particular, although it is commonly known that the silica nanoparticles can less significantly show the magnetic effect, we accomplished to use the silica nanoparticles as a signal regulator to ^{19}F NMR signals of the perfluorinated probes.

We developed the water-soluble perfluorinated dendrimers based on polyhedral oligomeric silsesquioxane.[66–81] The regulation system of ^{19}F NMR signals for monitoring bioreactions based on the silica nanoparticles is presented in Figure 14.[82] In a solid state, the sensitivity of NMR signal was suppressed by the acceleration of transverse relaxation time and the anisotropy of the spin toward the external magnetic fields. On silica NPs, the molecular rotation of the water-soluble perfluorinated dendrimers which is the signal unit for ^{19}F NMR detection should be highly restricted. At this state, the NMR signals from the dendrimer can be reduced. After releasing the dendrimer triggered by an enzymatic cleavage of the linker, the NMR signals should be recovered correspondingly by increasing the molecular motions. Thereby, the enzyme activity can be detected by the enhancement of the signal intensity of ^{19}F NMR.

(Figure 14)

To show the proof of concept, the detection with the dendrimer-coated silica

nanoparticles for alkaline phosphatase (AP) was demonstrated.[82] The reaction mixtures containing the modified nanoparticles and AP were incubated at 37 °C, and ^{19}F NMR signals from the mixture were monitored (Figure 15). The signal linearly increased until 12 h incubation (t_{50} = 6.2 h). In the absence of the enzyme, NMR signal was hardly observed even after 24 h incubation. These results indicate that the silica nanoparticles can work as a quencher for NMR signals. In addition, the AP activity can be detected by this system.

(Figure 15)

Bimodal probes for ^{19}F NMR/fluorescence detection

The quantitative analysis with the silica nanoparticle-based probes was carried out on the evaluation of the AP activity. We constructed the bimodal probes which can give the ^{19}F NMR signal and fluorescence simultaneously by the progress of the enzymatic reactions.[83] Such bimodal turn-on probes which offer simultaneous increases of the magnitudes of the respective signals between different modalities during the detections have potential advantages such as data reliability and yet also have potential limitations such as protein aggregation that affects both signaling systems. By replacing the linker to the phosphate-caged fluorescein, we examined the bimodal detection with ^{19}F NMR spectroscopy and fluorescence spectroscopy for the quantitative assay of an enzymatic reaction (Figure 16). The enzymatic reactions with AP were performed under the similar condition.[82] The signal changes were monitored in ^{19}F NMR and fluorescence. From the fitting to the standard line, the reaction yields were calculated as approximately 10% after 1 h incubation. On the other hand, signal intensities were continuously under

detection limit (less than 5% of the reaction yield) after 24 h incubation in the absence of AP. Next, we conducted the reactions by changing the concentrations of AP in the samples, and the signal intensities from the reaction mixtures were traced. The increases of the signal intensities were compared with the standard line prepared with the concentration-definitive dendrimer solutions and recalculated as the reaction yields. The increases of the yields calculated from ^{19}F NMR and fluorescence signals showed good agreement. From these data, it was suggested that enzymatic reaction can be assessed by the synchronized increases of fluorescence and ^{19}F NMR signals. In this system, different from the SPIO-based contrast agents, the interparticle interaction was not necessary for the target detection. Thus, our system could be feasible to receive the quantitative information under the intracellular circumstances. Furthermore, silica nanoparticles hardly disturb the optical properties of the coexisting dyes. As we demonstrated, silica nanoparticles are a versatile scaffold for fabricating the multimodal probes with optical functions.

(Figure 16)

Heavy metal-free NMR probes for evaluating glutathione reductase activity

The heavy metal species are not contained in our systems. Based on this property, we developed the ^{19}F NMR probes for evaluating the enzymatic activity which would be perturbed by heavy metals.[84] Glutathione reductase (GR) is a class of the NADPH-dependent enzyme which catalyzes the reduction of oxidized glutathione (GSSG) to GSH. The GSH production plays a central role in buffering an intercellular redox condition and in activating the anti-oxidation system.[85] In addition, it has been

reported that a significant enhancement of the GR activity was observed in malignant tumor cells.[86] Therefore, the quantification of the GR activity at the deep spot inside vital organs is of great significance for further understanding of the stress responses and carcinogenesis. The conventional assay for evaluating the GR activity is to follow the decrease in absorbance of NADPH at 340 nm.[87] Because of the low permeability of the light through a body, it is difficult to apply the conventional methods for the in vivo assay. Hence, the new methodology is desired for the quantitative analysis of the GR activity. Furthermore, the GR activity can be enhanced in the presence of heavy metal species. Thereby, the most of MR probes is not applicable since the probe itself should perturb the GR activity. Thus, we expected that our silica nanoparticle-based probes should be suitable for quantitatively measuring the GR activity with ^{19}F NMR.

Figure 17 illustrates the probe structure for measuring the GR activity.[84] The water-soluble perfluorinated dendrimers were immobilized onto the silica nanoparticles via the disulfide bond. By the cleavage of the linker, the perfluorinated dendrimer can be released, and the ^{19}F NMR signals are promised to be enhanced. Hence, the enzymatic reaction can be monitored by the increase of the signal molecule, perfluorinated dendrimers in ^{19}F NMR measurements. To test the reactivity of the probes, we performed the reactions with GSH, GSSG, and NADPH. The signals increased after incubation in the presence of $NaBH_4$, dithiothreitol (DTT), and GSH. These results indicate that the perfluorinated dendrimers can be released by reductive cleavage of disulfide bonds at the linker. On the other hand, both signals were hardly detected after the incubation in the presence of GSSG and NADPH. This means that coexisting molecules should less affect the linker cleavage. From these results, therefore

only the GR activity can be evaluated using our probe as the increase of ^{19}F NMR signals.

(Figure 17)

The feasibility of the probes was evaluated in the presence of the miscellaneous molecules under bio-mimetic conditions (Figure 18). The GR activity of the HeLa cell lysate was determined, and the results were compared to those from the conventional method. From the estimation calculated from the consumption rate of β-NADPH in the sample, the GR activity was determined as 0.61 ± 0.05 U/mL. Correspondingly, the GR activity of the sample was evaluated to be 0.65 ± 0.14 U/mL with our probes by fitting the signal increasing rates onto the standard curve. These data suggest that our NP probes can be applied for imaging the GR activity under the reductive environment in the cells with MRI.

(Figure 18)

The application of the silica nanoparticles as a heat generator is explained.[88] ILs have the ability of the efficient exothermal effect under the microwave irradiation.[89] Since the ionic conduction heating is generally much stronger than dipole rotation heating mechanism, the temperature of the aqueous solutions containing hydrophilic ILs increases much rapidly by the microwave irradiation. Based on these properties, if ILs can be localized in the target site inside bodies, the remote control of the heat generation can be realized by using the microwave irradiation. However, it is critically difficult to

deliver and sustain the ILs at the target spot inside the vital bodies. Thereby, we employed the silica nanoparticles as a scaffold for constructing the IL-based heat generators.

Heat generator under microwave irradiation

The imidazolium-presenting silica nanoparticles (Im-SiNPs) were prepared (Figure 19).[88] The synthesized nanoparticles showed good dispersibility in the aqueous media. Temperature profiles of the dispersions during microwave irradiation are shown in Figure 20. The rapid increase of the temperature of the sample containing Im-SiNPs was observed by +43 °C after 5 min irradiation. Subsequently, the increasing rate gradually reduced and reached a plateau. On the other hand, although the temperatures of the dispersion with unmodified silica nanoparticles increased, the initial rate until 2 min and the temperatures at 5 min were lower (SiNPs: +28 °C, blank: +26 °C) than those of Im-SiNPs. These results indicate that Im-SiNPs improved the increasing rate of the temperature under microwave irradiation. According to the series of measurements, it was summarized that the dielectric losses between imidazolium cations and water clusters should be mainly responsible for the heat generation under microwave irradiation to Im-SiNPs.

(Figures 19 and 20)

Gold nanoparticles

Cluster formation via anion exchange and unique optical properties

Gold nanoparticles (gold atoms; Au_n, $n < 100$) have the unique light absorption

properties originated from the coherent oscillation of the conduction band electrons (surface plasmon oscillation) induced by interaction with an electromagnetic field. In particular, the absorption properties are sensitively changed by the cluster formation.[90,91] To apply these characteristic optical properties of the gold nanoparticles for developing advanced materials, many studies have been made on the preparation of various shapes and the regulation of the dispersion states. For example, biosensors have been reported based on the cluster formation of gold nanoparticles for monitoring biological events or reactions. The interparticle forces including electrostatic[92], zwitterionic[93], van der Waals forces[94,95], as well as hydrogen bonding forces[96,97] have been utilized as a trigger for the cluster formation, and the highly-sensitive sensors were fabricated.[98] In the material science, the structural controls of the gold nanoparticles in the clusters have been focused. Since the precisely-ordered gold clusters are potential candidates for obtaining the advanced materials such as negative or low refractive indices, interparticle distances, distributions, and morphologies of gold nanoparticles after the cluster formation are vigorously explored.[99,100] In these studies, the interparticle distances are the key factor for the optical properties originated from the surface plasmon. In this part, we introduce the regulation of interparticle distances in the clusters of the gold nanoparticles.

We prepared the series of the modified gold nanoparticles covered with the imidazolium-containing ion pairs (Figure 21).[98] The substituent groups in imidazolium cation were replaced to ethylene oxide, methyl and butyl groups. The relationship between the chemical structures of the surface modification and the interparticle distances in the clusters was investigated. In addition, influence of anion exchange on the cluster formation and subsequently the optical properties was examined.

(Figure 21)

In summary, depended on the type of the additional anions, the interparticle distances obtained from the electronic microscopic observation can be modulated. Correspondingly, the absorption bands were altered. As a typical example, to the aqueous dispersion of the gold nanoparticles, same volume of the aqueous solutions containing KTFSI (TFSI = $(CF_3SO_2)_2N$) were added, and the time-courses of the changes of the optical properties were monitored with UV–vis absorption measurements. The peak tops of the surface plasmon bands from the gold nanoparticles shifted. The absorption band of the nanoparticles with ethylene oxide-substituted imidazolium showed slight bathochromic shift by +6 nm. In contrast, the nanoparticles with butyl-substituted imidazolium gave larger peak shift (+54 nm) by adding KTFSI. These changes can be also confirmed by naked eyes. The color of the aqueous dispersion containing the nanoparticles with butyl-substituted imidazolium turned to relatively purple. These data indicate that the interparticle distances should decrease corresponded to the hydrophobicities of the *N*-substituent in imidazolium. The similar results were obtained from the TEM images. It was found that the interparticle distances of the nanoparticles with methyl- and butyl-substituted imidazolium were 1.4 nm and 1.1 nm, respectively. Furthermore, the ethylene oxide-having nanoparticles showed a highly dispersion state. These data mean that the interparticle distances can be modulated at the sub-nano scale by regulating the hydrophobicity at the surface modification of the gold nanoparticles.

^{19}F NMR probes for detecting reduced glutathione triggered by heat activation

Gold nanoparticles can be a heat generator under the near-infrared light irradiation.[101] Temperature controls at the local spot can be achieved. Indeed, gold nanoparticles have been used in the clinical scene for anti-tumor treatments called hyperthermia.[101] Based on this ability as a heat generator, we developed the functional MR probes which can be activated by heating for realizing site- and time-specific analysis.[102]

As we mentioned above, it has been reported that the GSH concentrations are relatively higher in cancer cells than those in normal cells.[41–43] Therefore, GSH can be a marker of the active tumor.[39] GSH also plays significant another role in the metabolism. The existence of reactive oxygen or heavy metal species would be recognized as a stress to the cells, leading to the production of GSH.[44–46] Thus, the GSH-responsive materials are promised to be molecular probes for surveying stress-responses. The cellular distribution of GSH is commonly heterogeneous.[103] Furthermore, the GSH concentrations can be changed during biological events such as apoptosis via the transporting systems.[104] In addition, GSH can be found not only in the extracellular matrices but also in the blood.[105,106] Site- and time-specific analytical tools should be needed for evaluating the GSH concentration with high accuracy. To solve these problems, we designed the ^{19}F NMR probes having the heat-activation system: Before activation, the probes do not recognize GSH. After the heating treatment for the activation, the probe starts the detection. Finally, we expected that the increases of the signal can be observed, and the amount of GSH can be determined from the increasing rates as we demonstrated in the determination of AP and GR activities.

Figure 22 represents the structure and the detection mechanism for GSH in this study.[102] The probes consist of three components, the gold nanoparticle, the heat-cleavable linker, and the signal unit. The trifluoromethyl group is a ^{19}F NMR signal unit. The recognition of GSH is expected to provide the alteration of the chemical shift in ^{19}F NMR spectra. The reaction yields can be also evaluated from the peak ratio between before and after recognition. The thermally-cleavable linker possessed the adduct structures with maleimide and furan in a Diels–Alder reaction. At the initial state, the maleimide group is protected from the thiol group in GSH. After the heating activation, the retro Diels–Alder reaction proceeds. As a result, the maleimide group is exposure to GSH, leading to the Michael addition with the thiol group.[34] Finally, the electronic state of the trifluoromethyl group should be changed, and we can detect chemical-shift alteration in ^{19}F NMR spectra.

(Figure 22)

We synthesized the gold nanoparticle-based probes with the designed structure shown in Figure 22.[102] The suspension of the probes was heated at 90 °C, and ^{19}F NMR spectra were monitored. Before heating, the NMR signal was not observed from the probe. The molecular rotation of the trifluoromethyl groups should be highly restricted at the surface of the nanoparticles as we explained in the silica nanoparticle-based probes. After the thermal treatment at 90 °C for 10 min, ^{19}F NMR signal peak appeared at –73.4 ppm (Figure 23a). This result indicates that the signal unit was released from the surface of the nanoparticles. The reaction progress of Michael addition with GSH was monitored by the integral of peak area (Figure 23b). The conversion linearly increased

until 20 minutes incubation. We also examined the signal intensity of the sample without thermal treatment, the adducts of the probe with GSH were hardly detected in the ^{19}F NMR spectra. These results mean that the thermal activation to the probes can work as we expected. Based on this concept, the accuracy of the quantitative detection can be improved in the molecular imaging with the probe materials.

(Figure 23)

Synthesis

Typical synthetic protocol of SPIOs

Our preparation protocol for the SPIOs is described here:[27] To the solution containing iron(III) chloride hexahydrate (1.08 g, 4 mmol) and iron(II) chloride tetrahydrate (0.40 g, 2 mmol) in water (150 mL), 28% NH_4OH (15 mL) and 1 M citric acid in water (3 mL) were added, and the mixture was vigorously stirred by mechanical stirrer under nitrogen and then heated at 60 °C for 30 min. After the color changing from pale orange to black, the mixture was cooled to ambient temperature. The resultant SPIOs were collected with a magnet and washed with water three times. By treating with biotin, 5'-phosphorylated DNA and arsonoacetic acid, the modified SPIOs can be obtained. The preparation of the silica-coated core/shell type nanoparticles was performed with the oleic acid-presenting SPIOs.[58] In a 50 ml glass vial, 2.3 g of Igepal CO-520® was dissolved in 45 ml of cyclohexane. The solution was mechanically stirring at 700 rpm with sonication for 2 min. After dispersing the SPIO particles, 0.3 ml of the mixture was added to the cyclohexane solution, and then the mixture was stirred at room temperature for 5 min with sonication. The resulting mixture was turned to transparent light brown

liquid, and then 0.3 ml of tetraethoxysilane was added. The mixture was gently stirred by hand using spatura until tetraethoxysilane was completely dissolved, and the mixture was standed for 3 days at room temperature to form thick silica shell. Then, in 1000 ml of a round-bottom flask, the imidazolium[23] (2.0 g) was dissolved in 200 ml of ethanol. The mixture containing the core/shell particles was rapidly added to the ethanol solution with mechanically stirring at 700 rpm. After the mixture was stirred for 12 hours at room temperature, the upper transparent layer was removed, and the light-brown-colored products were separated by centrifuging at 6000 rpm. After washing with 200 ml of methanol in three times, the desired core/shell particles were obtained as a brown suspension in methanol. The diameters of the SPIOs were evaluated from the TEM images and the DLS spectra data. The existence of imidazolium to the SPIOs was confirmed from the IR spectra.

Preparation of modified silica nanoparticles

The modified silica nanoparticles for evaluating GR activity were prepared according to the previous report:[84] A solution containing 2 mL of tetraethoxysilane, 1 mL of 3-aminopropyltriethoxysilane, 7 mL of water, and 2 mL of ammonium hydroxide in 50 mL of ethanol was stirred at ambient temperature for 16 h, and then the white precipitate was separated by centrifugation. After washing with ethanol three times, the particles (152 ± 11 nm diameter) were obtained as a white powder. To determine the amounts of the reactive amino groups at the surface of the particles, we treated the silica nanoparticles with ethyl trifluoroacetate. After washing with methanol, the particles were dissolved in 1 *N* aqueous sodium hydroxide, and the peak height was compared to the standard samples. Consequently, it was found that 960 nmol of trifluoroacetyl

groups were attached to the particles. To the solution of the *N*-hydroxysccinimidyl ester[84] (404 mg. 1 mmol) and triethylamine (1 mL) in dichloromethane, 100 mg of amino-presented silica nanoparticles were added. After 1 h stirring at room temperature, nanoparticles were centrifuged and washed with dichloromethane. After drying *in vacuo*, the solution of the fluorinated dendrimer and triethylamine in methanol was added. The mixture was stirred at room temperature under ultrasound irradiation. After 1 h stirring, the nanoparticles were centrifuged and washed with methanol and dichloromethane. The white powder was obtained after drying (167 ± 10 nm diameter from TEM). To estimate the amount of the fluorinated dendrimer on the nanoparticles (18 nmol/mg, F atom: 216 nmol/mg), the ^{19}F NMR spectrum of the solution containing the nanoparticle probe dissolved in 1 *N* aqueous sodium hydroxide was compared to the spectra of the standard samples with various concentrations of trifluoroacetic acid.

Preparation of gold nanoparticles

A typical procedure is described as follows:[98] To a 50 mL screw bottle, the aqueous solution of $HAuCl_4$ (10.0 mg / 5 mL) and the thiol compound (0.012 mmol / 5 mL) were added to give the turbid orange solution. To the mixture, the aqueous solution of $NaBH_4$ (2.7 mg / 5 mL) was added slightly (5 mL/min) with vigorous stirring. The color of the solution immediately turned to dark red indicating the formation of gold nanoparticles. After stirring for 1 h, the mixture was filtered through the ultra-filtration membrane (ADVANTEC USY-5, MWCO = 50,000) and washed with distilled water several times to remove free imidazolium species and salts.

Conclusion:

We review a part of recent studies on the usages of nanoparticles in nanobiotechnology. By employing nanoparticles, we can easily receive the material properties based on the preprogrammed design on the chemical structures at the nanometer size. It was demonstrated that the cluster formations of SPIOs and gold nanoparticles can be freely controlled by the addition of various kinds of biomolecules or environmental factors. The silica nanoparticles can work as a regulator for NMR signals. As we introduce in this manuscript, nanoparticles are attractive candidates as a building block for fabricating bio-related materials. Moreover, in material science, the further functions of the nanoparticles concerning non-linear optics or electronics have been found more recently. We have numerous potentials for obtaining advanced functional materials based on these properties.

References:

[1] G. Kong, R.D. Braun, M.W. Dewhirst, Hyperthermia enables tumor-specific nanoparticle delivery: Effect of particle size, Cancer Research, 60 (2000) 4440-4445.

[2] O. Ishida, K. Maruyama, K. Sasaki, M. Iwatsuru, Size-dependent extravasation and interstitial localization of polyethyleneglycol liposomes in solid tumor-bearing mice, International Journal of Pharmaceutics, 190 (1999) 49-56.

[3] D.C. Litzinger, A.M. Buiting, N. van Rooijen, L. Huang, Effect of liposome size on the circulation time and intraorgan distribution of amphipathic poly(ethylene glycol)-containing liposomes, Biochimica et Biophysica Acta - Biomembranes, 1190 (1994) 99-107.

[4] F. Yuan, M. Leunig, S.K. Huang, D.A. Berk, D. Papahadjopoulos, R.K. Jain, Microvascular permeability and interstitial penetration of sterically stabilized (stealth) liposomes in a human tumor xenograft, Cancer Research, 54 (1994) 3352-33566.

[5] S.K. Hobbs, W.L. Monsky, F. Yuan, W.G. Roberts, L. Griffith, V.P. Torchilin, R.K. Jain, Regulation of transport pathways in tumor vessels: Role of tumor type and microenvironment, Proceedings of the National Academy of Sciences of the United States of America, 95 (1998) 4607-4612.

[6] H. Maeda, The enhanced permeability and retention (EPR) effect in tumor vasculature: The key role of tumor-selective macromolecular drug targeting, Advances in Enzyme Regulation, 41 (2001) 189-207.

[7] H. Maeda, J. Fang, T. Inutsuka, Y. Kitamoto, Vascular permeability enhancement in solid tumor: Various factors, mechanisms involved and its implications, International Immunopharmacology, 3 (2003) 319-328.

[8] S. Laurent, D. Forge, M. Port, A. Roch, C. Robic, L. Vander Elst, R.N. Muller, Magnetic iron oxide nanoparticles: Synthesis, stabilization, vectorization, physicochemical characterizations and biological applications, Chemical Reviews, 108 (2008) 2064-2110.

[9] L.H. Reddy, J.L. Arias, J. Nicolas, P. Couvreur, Magnetic nanoparticles: Design and characterization, toxicity and biocompatibility, pharmaceutical and biomedical applications, Chemical Reviews, 112 (2012) 5818-5878.

[10] K.E. Sapsford, W.R. Algar, L. Berti, K.B. Gemmill, B.J. Casey, E. Oh, M.H. Stewart, I.L. Medintz, Functionalizing nanoparticles with biological molecules: Developing chemistries that facilitate nanotechnology, Chemical Reviews, 113 (2013) 1904-2074.

[11] P. Samokhvalov, M. Artemyev, I. Nabiev, Basic principles and current trends in colloidal synthesis of highly luminescent semiconductor nanocrystals, Chemistry – A European Journal, 19 (2013) 1534-1546.

[12] H. Yukawa, M. Watanabe, N. Kaji, Y. Okamoto, M. Tokeshi, Y. Miyamoto, H. Noguchi, Y. Baba, S. Hayashi, Monitoring transplanted adipose tissue-derived stem cells combined with heparin in the liver by fluorescence imaging using quantum dots, Biomaterials, 33 (2012) 2177-2186.

[13] H. Yukawa, Y. Kagami, M. Watanabe, K. Oishi, Y. Miyamoto, Y. Okamoto, M. Tokeshi, N. Kaji, H. Noguchi, K. Ono, M. Sawada, Y. Baba, N. Hamajima, S. Hayashi, Quantum dots labeling using octa-arginine peptides for imaging of adipose tissue-derived stem cells, Biomaterials, 31 (2010) 4094-4103.

[14] J.W.M. Bulte, D.L. Kraitchman, Iron oxide MR contrast agents for molecular and cellular imaging, NMR in Biomedicine, 17 (2004), 484-499.

[15] A.S. Arbab, L.A. Bashaw, B.R. Miller, E.K. Jordan, J.W.M. Bulte, J.A. Frank, Intracytoplasmic tagging of cells with ferumoxides and transfection agent for cellular magnetic resonance imaging after cell transplantation: Methods and techniques, Transplantation, 76 (2003) 1123-1130.

[16] C. Corot, P. Robert, J.M. Idee, M. Port, Recent advances in iron oxide nanocrystal technology for medical imaging, Advanced Drug Delivery Reviews, 58 (2006) 1471-1504.

[17] J.A. Frank, B.R. Miller, A.S. Arbab, H.A. Zywicke, E.K. Jordan, B.K. Lewis, L.H. Bryant, Jr. J.W.M. Bulte, Clinically applicable labeling of mammalian and stem cells by combining superparamagnetic iron oxides and transfection agents, Radiology, 228 (2003) 480-487.

[18] C. Wilhelm, F. Gazeau, Universal cell labelling with anionic magnetic nanoparticles, Biomaterials, 29 (2008) 3161-3174.

[19] E. Katz, I. Willner, Integrated nanoparticle-biomolecule hybrid systems: Synthesis, properties, and applications, Angewandte Chemie - International Edition, 43 (2004) 6042-6108.

[20] J.M. Perez, L. Josephson, R. Weissleder, Use of magnetic nanoparticles as nanosensors to probe for molecular interactions, ChemBioChem, 5 (2004) 261-264.

[21] M.V. Yigit, D. Mazumdar, H.K. Kim, J.H. Lee, B. Odintsov, Y. Lu, Smart "turn-on" magnetic resonance contrast agents based on aptamer-functionalized superparamagnetic iron oxide nanoparticles, ChemBioChem, 8 (2007) 1675-1678.

[22] T. Atanasijevic, A. Jasanoff, Preparation of iron oxide-based calcium sensors for MRI, Nature protocols, 2 (2007) 2582-2589.

[23] Z. Medarova, W. Pham, C. Farrar, V. Petkova, A. Moore, In vivo imaging of siRNA

delivery and silencing in tumors, Nature Medicine, 13 (2007) 372-377.

[24] M. Lewin, N. Carlesso, C.H. Tung, X.W. Tang, D. Cory, D.T Scadden,. R. Weissleder, Tat peptide-derivatized magnetic nanoparticles allow in vivo tracking and recovery of progenitor cells, Nature Biotechnology, 18 (2000) 410-414.

[25] C. Sun, J.S.H. Lee, M. Zhang, Magnetic nanoparticles in MR imaging and drug delivery, Advanced Drug Delivery Reviews, 60 (2008) 1252-1265.

[26] Y.M. Huh, Y.W. Jun, H.T. Song, S. Kim, J.S. Choi, J.H. Lee, S. Yoon, K.S. Kim, J.S. Shin, J.S. Shu, J. Cheon, In vivo magnetic resonance detection of cancer by using multifunctional magnetic nanocrystals, Journal of the American Chemical Society, 127 (2005) 12387-12391.

[27] K. Tanaka, N. Kitamura, M. Morita, T. Inubushi, Y. Chujo, Assembly system of direct modified superparamagnetic iron oxide nanoparticles for target-specific MRI contrast agents, Bioorganic and Medicinal Chemistry Letters, 18 (2008) 5463-5465.

[28] Y. Li, D. Sen, A catalytic DNA for porphyrin metallation, Nature Structural Biology, 3 (1996) 743-747.

[29] N. Nasongkla, E. Bey, J. Ren, H. Ai, C. Khemtong, J.S. Guthi, S.F. Chin, A.D. Sherry, D.A. Boothman, J. Gao, Multifunctional polymeric micelles as cancer-targeted, MRI-ultrasensitive drug delivery systems, Nano Letters, 6 (2006) 2427-2430.

[30] J.L. Wike-Hooley, J. Haveman, H.S. Reinhold, The relevance of tumour pH to the treatment of malignant disease, Radiotherapy and Oncology, 2 (1984) 343-366.

[31] L.E. Gerweck, K. Seetharaman, Cellular pH gradient in tumor versus normal tissue: Potential exploitation for the treatment of cancer, Cancer Research, 56 (1996) 1194-1198.

[32] J. Gruenberg, The endocytic pathway: A mosaic of domains, Nature Reviews

Molecular Cell Biology, 2 (2001) 721-730.

[33] S. Mukheriee, R.N. Ghosh, F.R. Maxfield, Endocytosis, Physiological Reviews, 77 (1997) 759-803.

[34] Y. Shiraishi, D. Arakawa, N. Toshima, pH-dependent color change of colloidal dispersions of gold nanoclusters: Effect of stabilizer, European Physical Journal E, 8 (2002) 377-383.

[35] J. Simard, C. Briggs, A.K. Boal, V.M. Rotello, Formation and pH-controlled assembly of amphiphilic gold nanoparticles, Chemical Communications, (2000) 1943-1944.

[36] D.G. Fatouros, P. Klepetsanis, P.V. Ioannou, S.G. Antimisiaris, The effect of pH on the electrophoretic behaviour of a new class of liposomes: Arsonoliposomes, International Journal of Pharmaceutics, 288 (2005) 151-156.

[37] H. Minehara, K. Naka, K. Tanaka, A. Narita, Y. Chujo, Arsonic acid-presenting superparamagnetic iron oxide for pH-responsive aggregation under slightly acidic conditions, Bioorganic and Medicinal Chemistry, 19 (2011) 2282-2286.

[38] H. Minehara, A. Narita, K. Naka, K. Tanaka, M. Chujo, M. Nagao, Y. Chujo, Tumor cell-specific prodrugs using arsonic acid-presenting iron oxide nanoparticles with high sensitivity, Bioorganic and Medicinal Chemistry, 20 (2012) 4675-4679.

[39] K. Tanabe, H. Harada, M. Narazaki, K. Tanaka, K. Inafuku, H. Komatsu, T. Ito, H. Yamada, Y. Chujo, T. Matsuda, M. Hiraoka, S. Nishimoto, Monitoring of biological one-electron reduction by ^{19}F NMR using hypoxia selective activation of an ^{19}F-labeled indolequinone derivative, Journal of the American Chemical Society, 131 (2009) 15982-15983.

[40] N. Hirata, K. Tanabe, A. Narita, K. Tanaka, K. Naka, Y. Chujo, S. Nishimoto,

Preparation and fluorescence properties of fluorophore-labeled avidin-biotin system immobilized on Fe_3O_4 nanoparticles through functional indolequinone linker, Bioorganic and Medicinal Chemistry, 17 (2009) 3775-3781.

[41] C. Murakami, Y. Hirakawa, H. Inui, Y. Nakano, H. Yoshida, Effect of tea catechins on cellular lipid peroxidation and cytotoxicity in HepG2 cells, Bioscience, Biotechnology and Biochemistry, 66 (2002) 1559-1562.

[42] H. Toyoda, T. Mizushima, M. Satoh, N. Iizuka, A. Nomoto, H. Chiba, M. Mita, A. Naganuma, S. Himeno, N. Imura, HeLa cell transformants overproducing mouse metallothionein show in vivo resistance to cis-platinum in nude mice, Japanese Journal of Cancer Research, 91 (2000) 91-98.

[43] S. Ueno, N. Susa, Y. Furukawa, K. Aikawa, I. Itagaki, T. Komiyama, Y. Takashima, Effect of Chromium on Lipid Peroxidation in Isolated Rat Hepatocytes, The Japanese Journal of Veterinary Science, 50 (1988) 45-52.

[44] S.M. Deneke, B.L. Fanburg, Regulation of cellular glutathione, American Journal of Physiology, 257 (1989) L163-L173.

[45] O. Carmel-Harel, G. Storz, Roles of the glutathione- and thioredoxin-dependent reduction systems in the Escherichia coli and Saccharomyces cerevisiae responses to oxidative stress, Annual Review of Microbiology, 54 (2000) 439-461.

[46] J. Nordberg, E.S. Arnér, Reactive oxygen species, antioxidants, and the mammalian thioredoxin system, Free Radical Biology and Medicine, 31 (2001) 1287-1312.

[47] P.V. Ioannou, On the direct reduction of arsonic acids to arsenoso compounds: Mechanisms and preparations, Applied Organometallic Chemistry, 14 (2000) 261-272.

[48] M.A. Lala, P.V. Ioannou, The reaction of allyl and benzylarsonic acids with thiols: Mechanistic aspects and implications for dioxygen activation by trivalent arsenic

compounds, Journal of Inorganic Biochemistry, 97 (2003) 331-339.

[49] O. Gortzi, S.G. Antimisiaris, P. Klepetsanis, E. Papadimitriou, P.V. Ioannou, Arsonoliposomes: Effect of arsonolipid acyl chain length and vesicle composition on their toxicity towards cancer and normal cells in culture, European Journal of Pharmaceutical Sciences, 18 (2003) 175-183.

[50] O. Gortzi, E. Papadimitriou, C.G. Kontoyannis, S.G. Antimisiaris, P.V. Ioannou, Arsonoliposomes, a novel class of arsenic-containing liposomes: Effect of palmitoyl-arsonolipid-containing liposomes on the viability of cancer and normal cells in culture, Pharmaceutical Research, 19 (2002) 79-86.

[51] K. Naka, A. Narita, H. Tanaka, Y. Chujo, M. Morita, T. Inubushi, I. Nishimura, J. Hiruta, H. Shibayama, M. Koga, S. Ishibashi, J. Seki, S. Kizaka-Kondoh, M. Hiraoka, Biomedical applications of imidazolium cation-modified iron oxide nanoparticles, Polymers for Advanced Technologies, 19 (2008) 1421-1429.

[52] A. Narita, K. Naka, Y. Chujo, Facile control of silica shell layer thickness on hydrophilic iron oxide nanoparticles via reverse micelle method, Colloids Surf. A 336 (2009) 46-56.

[53] K. Naka, H. Tanaka, Y. Chujo, pH responsive aggregation of imidazolium cations-modified gold nanoparticles with poly(acrylic acid) in aqueous solution, Polymer Journal, 39 (2007) 1122-1127.

[54] H. Itoh, K. Naka, Y. Chujo, Synthesis of gold nanoparticles modified with ionic liquid based on the imidazolium cation, Journal of the American Chemical Society, 126 (2004) 3026-3027.

[55] K. Tanaka, A. Narita, K. Suzuki, Y. Chujo, Regulation of dispersion/aggregation of phosphonium-presenting iron oxide nanoparticles by anion exchange, Composite

Interfaces, 20 (2013) 557-564.

[56] K. Tanaka, A. Narita, Y. Chujo, Catch and release with DNA by imidazolium-presenting iron oxide nanoparticles via anion exchange, Composite Interfaces, 20 (2013) 27-32.

[57] M. Uhlen, Magnetic separation of DNA, Nature 340 (1989) 733-734.

[58] K. Tanaka, A. Narita, N. Kitamura, W. Uchiyama, M. Morita, T. Inubushi, Y. Chujo, Preparation for highly-sensitive MRI contrast agents using core/shell type nanoparticles consisted of multiple SPIO cores with thin silica coating, Langmuir 26 (2010) 11759-11762.

[59] X. Sun, S.M. Tabakman, W.S. Seo, L. Zhang, G. Zhang, S. Sherlock, L. Bai, H. Dai, Separation of nanoparticles in a density gradient: FeCo@C and gold nanocrystals, Angewandte Chemie - International Edition, 48 (2009) 939-942.

[60] J.H. Lee,; Y.M. Huh, Y.W. Jun, J.W. Seo, J.T. Jang, H.T. Song, S. Kim, E.J. Cho, H.G. Yoon, J.S. Suh, Artificially engineered magnetic nanoparticles for ultra-sensitive molecular imaging, Nature Medicine, 13 (2007) 95-99.

[61] W. Stöber, A. Fink, E. Bohn, Controlled growth of monodisperse silica spheres in the micron size range, Journal of Colloid And Interface Science, 26 (1968) 62-69.

[62] A. Burns, H. Ow, U. Wiesner, Fluorescent core-shell silica nanoparticles: Towards "lab on a particle" architectures for nanobiotechnology, Chemical Society Reviews, 35 (2006) 1028-1042.

[63] Reversible signal regulation system of ^{19}F NMR by redox reactions using a metal complex as a switching module, Bioorganic and Medicinal Chemistry, 17 (2009) 3818-3823.

[64] N. Kitamura, T. Hiraoka, K. Tanaka, Y. Chujo, Reduced glutathione-resisting ^{19}F

NMR sensors for detecting HNO, Bioorganic and Medicinal Chemistry, 20 (2012) 4675-4679.

[65] K. Tanaka, K. Inafuku, Y. Chujo, Ratiometric multimodal chemosensors based on cubic silsesquioxanes for monitoring solvent polarity, Bioorganic and Medicinal Chemistry, 16 (2008) 10029-10033.

[66] K. Tanaka, Y. Chujo, Advanced functional materials based on polyhedral oligomeric silsesquioxane (POSS), Journal of Materials Chemistry, 22 (2012) 1733-1746.

[67] K. Tanaka, Y. Chujo, Unique properties of amphiphilic POSS and their applications, Polymer Journal, 45 (2013) 247-254.

[68] K. Tanaka, S. Adachi, Y. Chujo, Structure-property relationship of octa-substituted POSS in thermal and mechanical reinforcements of conventional polymers, Journal of Polymer Science, Part A: Polymer Chemistry, 47 (2009) 5690-5697.

[69] K. Tanaka, S. Adachi, Y. Chujo, Side-chain effect of octa-substituted POSS fillers on refraction in polymer composites, Journal of Polymer Science, Part A: Polymer Chemistry, 48 (2010) 5712-5717.

[70] K. Tanaka, F. Ishiguro, Y. Chujo, POSS ionic liquid, Journal of the American Chemical Society, 132 (2010) 17649-17651.

[71] K. Tanaka, F. Ishiguro, Y. Chujo, Thermodynamic study of POSS-based ionic liquids with various numbers of ion pairs, Polymer Journal, 43 (2011) 708-713.

[72] K. Tanaka, N. Kitamura, K. Naka, M. Morita, T. Inubushi, M. Chujo, M. Nagao, Y. Chujo, Improving proton relaxivity of dendritic MRI contrast agents by rigid silsesquioxane core, Polymer Journal, 41 (2009) 287-292.

[73] K. Tanaka, K. Inafuku, Y. Chujo, Tuning of properties of POSS-condensed

water-soluble network polymers by modulating the cross-linking ratio between POSS, Macromolecules, 42 (2009) 3489-3492.

[74] K. Tanaka, W. Ohashi, N. Kitamura, Y. Chujo, Reductive glutathione-responsive molecular release using water-soluble POSS network polymers, Bulletin of the Chemical Society of Japan, 84 (2011) 612-616.

[75] J.H. Jeon, K. Tanaka, Y. Chujo, POSS Fillers for Modulating Thermal Properties of Ionic Liquids, RSC Advances, 3 (2013) 2422-2427.

[76] K. Tanaka, J.H. Jeon, K. Inafuku, Y. Chujo, Enhancement of optical properties of dyes for bioprobes by freezing effect of molecular motion using POSS-core dendrimers, Bioorganic and Medicinal Chemistry, 20 (2012) 915-919.

[77] K. Tanaka, M. Murakami, J.H. Jeon, Y. Chujo, Enhancement of affinity in molecular recognition via hydrogen bonds by POSS-core dendrimer and its application for selective complex formation between guanosine triphosphate and 1,8-naphthyridine derivatives, Organic and Biomolecular Chemistry, 10 (2012) 90-95.

[78] K. Tanaka, K. Inafuku, K. Naka, Y. Chujo, Enhancement of entrapping ability of dendrimers by a cubic silsesquioxane core, Organic and Biomolecular Chemistry, 6 (2008) 3899-3901.

[79] K. Naka, M. Fujita, K. Tanaka, Y. Chujo, Water-soluble anionic POSS-core dendrimer: synthesis and copper(II) complexes in aqueous solution, Langmuir, 23 (2007) 9057-9063.

[80] K. Tanaka, K. Inafuku, Y. Chujo, Environment-responsive upconversion based on dendrimer-supported efficient triplet-triplet annihilation in aqueous media, Chemical Communications, 46 (2010) 4378-4380.

[81] K. Tanaka, H. Okada, J.H. Jeon, K. Inafuku, W. Ohashi, Y. Chujo, Hypoxic

conditions-selective upconversion via triplet-triplet annihilation based on POSS-core dendrimer complexes, Bioorganic and Medicinal Chemistry, 21 (2013) 2678-2681.

[82] K. Tanaka, N. Kitamura, K. Naka, Y. Chujo, Multi-modal ^{19}F NMR probe using perfluorinated cubic silsesquioxane-coated silica nanoparticles for monitoring enzymatic activity, Chemical Communications, (2008) 6176-6178.

[83] K. Tanaka, N. Kitamura, Y. Chujo, Bimodal quantitative monitoring for enzymatic activity with simultaneous signal increases in ^{19}F NMR and fluorescence using silica nanoparticle-based molecular probes, Bioconjugate Chemistry, 22 (2011) 1484-1490.

[84] K. Tanaka, N. Kitamura, Y. Chujo, Heavy metal-free ^{19}F NMR probes for quantitative measurements of glutathione reductase activity using silica nanoparticles as a signal quencher, Bioorganic and Medicinal Chemistry, 20 (2012) 96-100.

[85] J. Nordberg, E.S.J. Arnér, Reactive oxygen species, antioxidants, and the mammalian thioredoxin system, Free Radical Biology and Medicine, 31 (2001) 1287-1312.

[86] H. Malmgren, B. Sylvén, The histological distribution of glutathione reductase activity in solid mouse tumor transplants and a comparison with ascites tumors and normal tissues, Cancer research, 20 (1960) 204-211.

[87] F. Tietze, Enzymic method for quantitative determination of nanogram amounts of total and oxidized glutathione: Applications to mammalian blood and other tissues, Analytical Biochemistry, 27 (1969) 502-522.

[88] H. Okada, Y. Kajiwara, K. Tanaka, Y. Chujo, Rapid heat generation under microwave irradiation by imidazolium-presenting silica nanoparticles, Colloids and Surfaces A: Physicochemical and Engineering Aspects, 428 (2013) 65–69.

[89] P. Lindström, J. Tierney, B. Wathey, J. Westman, Microwave assisted organic

synthesis, Tetrahedron, 57 (2001) 9225–9283.

[90] M.C. Daniel, D. Astruc, Gold nanoparticles: assembly, supramolecular chemistry, quantum-size-related properties, and applications toward biology, catalysis, and nanotechnology, Chemical Reviews, 104 (2004) 293-346.

[91] R. Shenhar, V.M. Rotello, Nanoparticles: scaffolds and building blocks, Account of Chemical Research, 36 (2003) 549-561.

[92] S. Zhang, X. Kou, Z. Yang, Q. Shi, G.D. Stucky, L. Sun, J. Wang, C. Yan, Nanoneckles assembled from gold rods, spheres, and bipyramids, Chemical Communications, (2007) 1816-1818.

[93] I.I.S. Lim, W. Ip, E. Crew, P.N. Njoki, D. Mott, C.J. Zhong, Y. Pan, S. Zhou, Homocysteine-mediated reactivity and assembly of gold nanoparticles, Langmuir, 23 (2007) 826-833.

[94] L. Han, J. Luo, N. Kariuki, M.M. Maye, V.W. Jones, C.J. Zhong, Novel interparticle spatial properties of hydrogen-bonding mediated nanoparticle assembly, Chemistry of Materials, 15 (2003) 29-37.

[95] J.B. Carroll, B.L. Frankamp, V.M. Rotello, Self-assembly of gold nanoparticles through tandem hydrogen bonding and polyoligosilsequioxane (POSS)–POSS recognition processes, Chemical Communications (2002) 1892-1893.

[96] W. Zheng, M.M. Maye, F.L. Leibowitz, C.J. Zhong, Imparting biomimetic ion-gating recognition properties to electrodes with a hydrogen-bonding structured core-shell nanopartricle network, Analytical Chemistry, 72 (2000) 2190-2199.

[97] I.I.S. Lim, D. Mott, W. Ip, P.N. Njoki, Y. Pan, S. Zhou, C.J. Zhong, Interparticle interactions of glutathione mediated assembly of gold nanoparticles, Langmuir, 24 (2008) 8857-8863.

[98] E. Miyoshi, K. Naka, K. Tanaka, A. Narita, Y. Chujo, Preparation of clusters having various interparticle distances based on imidazolium-modified gold nanoparticles via anion exchange, Colloids and Surfaces A: Physicochemical and Engineering Aspects, 390 (2011) 126-133.

[99] S. Kubo, A. Diaz, Y. Tang, T.S. Mayer, I.C. Khoo, T.E. Mallouk, Tunability of the refractive index of gold nanoparticle dispersions, Nano Letters, 7 (2007) 3418-3423

[100] S.K. Ghosh, T. Pal, Interparticle coupling effect on the surface plasmon resonance of gold nanoparticles: from theory to applications, Chemical Reviews, 107 (2007) 4797-4862.

[101] R.A. Sperling, P. Riveragil, F. Zhang, M. Zanella, W.J. Parak, Biological applications of gold nanoparticles, Chemical Society Reviews, 37 (2008) 1896-1908.

[102] N. Kitamura, K. Tanaka, Y. Chujo, Heat-initiated detection for reduced glutathione

with ^{19}F NMR probes based on modified gold nanoparticles, Bioorganic and Medicinal Chemistry Letters, 23 (2013) 281-286.

[103] L.H. Lash, T.M. Visarius, J.M. Sall, W. Qian, J.J. Tokarz, Cellular and subcellular heterogeneity of glutathione metabolism and transport in rat kidney cells, Toxicology, 130 (1998) 1-15.

[104] L.H. Lash, Role of glutathione transport processes in kidney function, Toxicology and Applied Pharmacology, 204 (2005) 329-342.

[105] Y. Yamada, Y. Tani, T. Kamihara, Production of extracellular glutathione by Candida tropicalis Pk 233, Journal of General Microbiology, 130 (1984) 3275-3278.

[106] J. Behr, B. Degenkolb, K. Maier, B. Braun, T. Beinert, F. Krombach, C. Vogelmeier, G. Fruhmann, Increased oxidation of extracellular glutathione by

bronchoalveolar inflammatory cells in diffuse fibrosing alveolitis, European Respiratory Journal, 8 (1995) 1286-1292.

Figures:

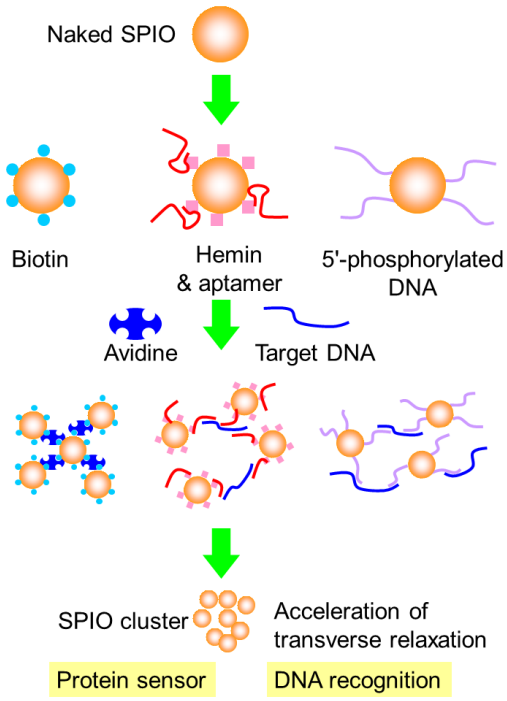

Figure 1. Schematic illustrations for the biomolecule-triggered cluster formations of the modified SPIOs.

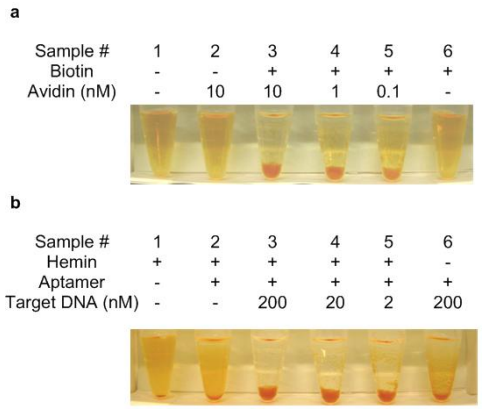

Figure 2. The cluster formation of (a) the biotin-presenting and (b) the hemin-aptamer DNA complex-modified SPIOs by the addition of each target molecule in the buffer. All images were taken after 15 min standing (+: added to the samples).

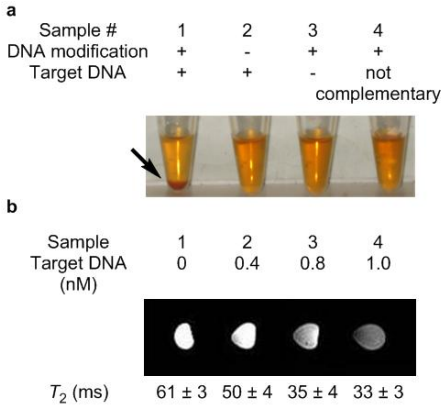

Figure 3. The cluster formation of the DNA-presenting SPIOs by adding the target DNA in the buffer. (a) Images were taken after 15 min standing. (b) T_2-weighted coronal MRI image and their relaxation times.

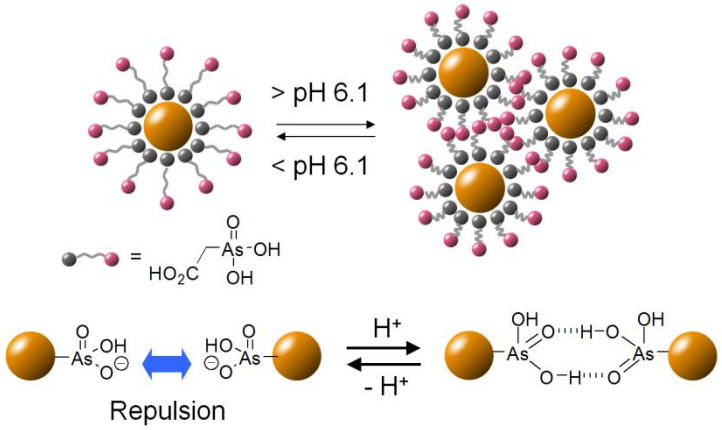

Figure 4. Plausible model for the reversible switching of dispersion/aggregation of the arsonic acid-presenting SPIOs by pH alteration.

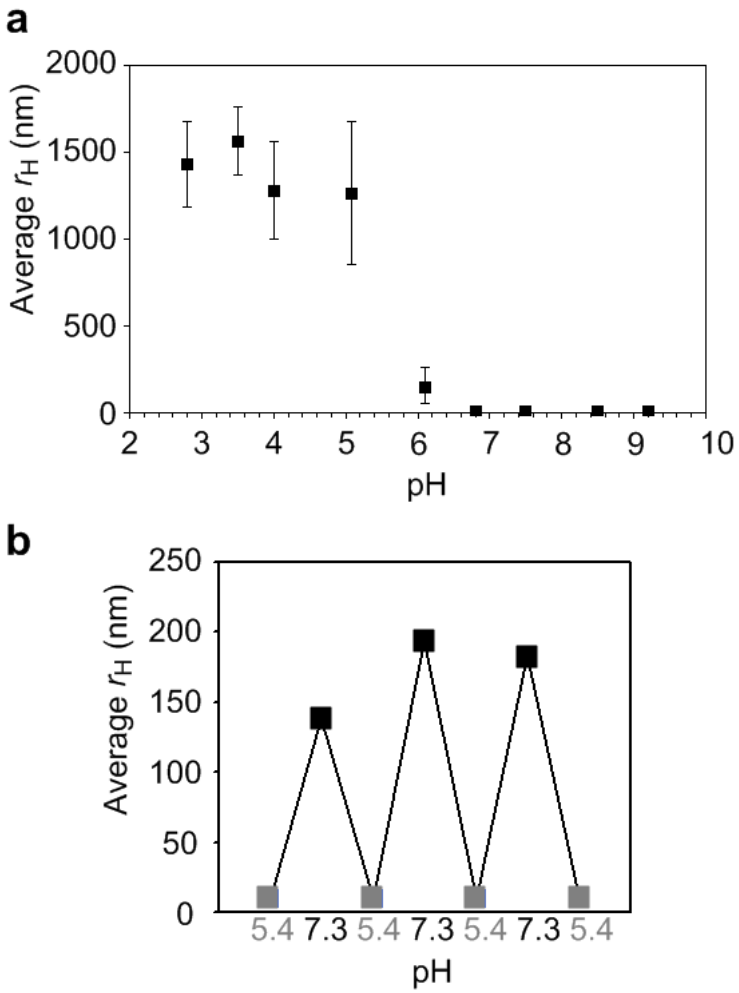

Figure 5. (a) The pH-dependent aggregation of the arsonic acid-presenting SPIOs. (b) Reversibility of pH-responsive assembly of the arsonic acid-presenting SPIOs.

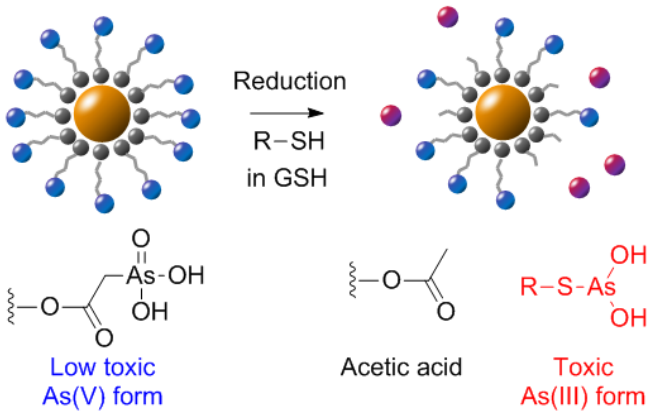

Figure 6. Proposed reaction scheme of the reduction of arsonoacetic acid with GSH.

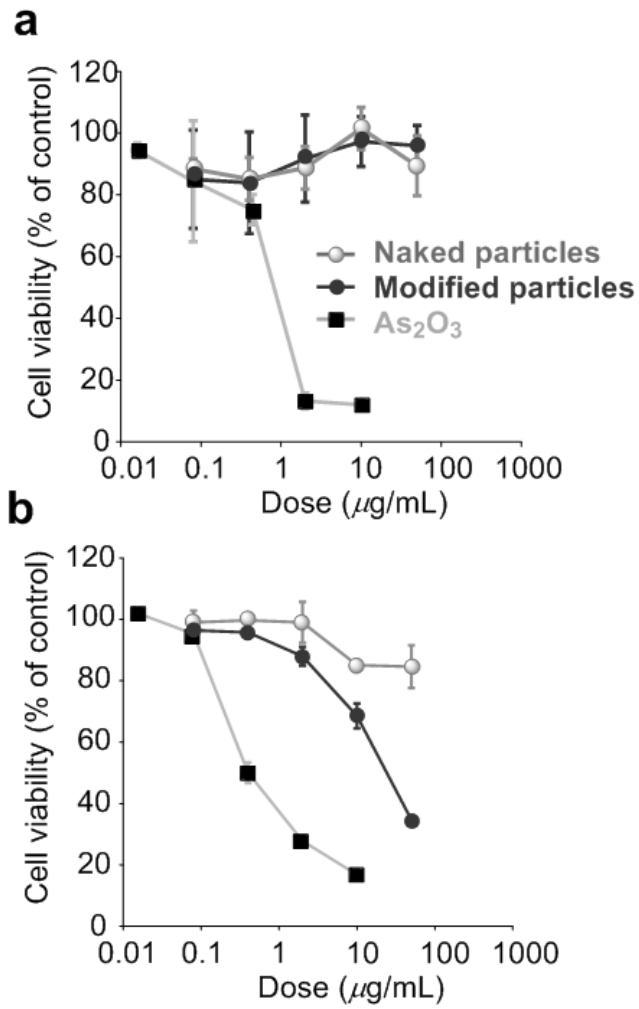

Figure 7. Effect of As_2O_3, naked iron oxide nanoparticles, and the modified nanoparticles on the viability of (a) primary mouse hepatocytes and (b) tumor cell line (HepG2). Cells were incubated with various concentrations of the samples for 72 h. Results are expressed as viability (% viable cells in comparison with the control) versus the arsenic content for upper three graphs.

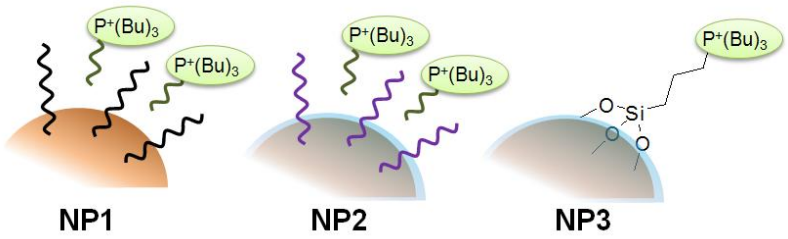

Figure 8. Structures of the phosphonium-presenting SPIOs.

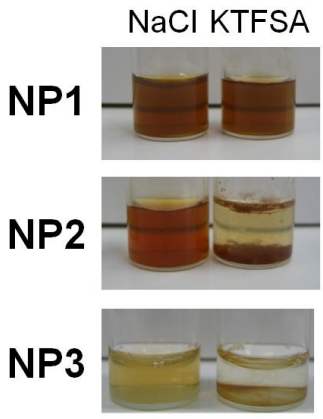

Figure 9. Pictures of the dispersions of the phosphonium-presenting SPIOs after adding NaCl and KTFSA.

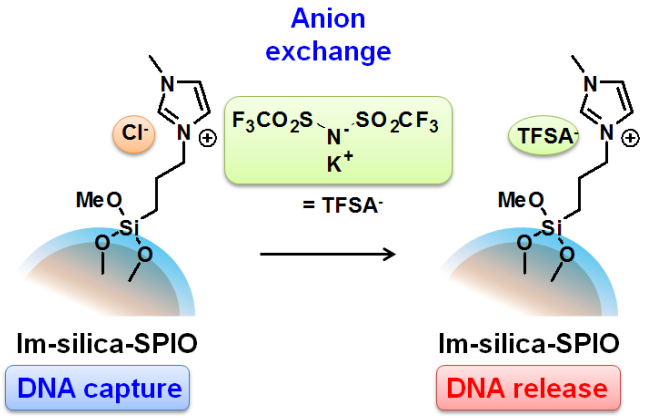

Figure 10. Outlines of the DNA catch and release by the imidazolium-presenting SPIOs.

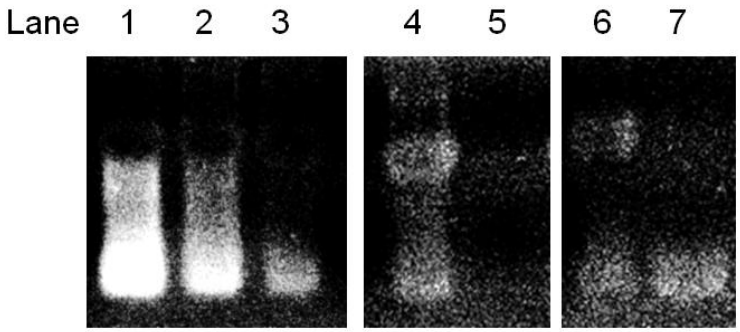

Figure 11. The release of the plasmid DNA from the Im-SPIOs via anion exchange. Lane 1, 2.5 μg of DNA; lane 2, 1 μg of DNA; lane 3, 0.5 μg of DNA; lane 4, the supernatant containing 2.5 μg of DNA and 50 μg of Im-SPIOs; lane 5, the supernatant after adding 0.5 M KCl to the DNA-adsorbed Im-SPIOs; lane 6, the supernatant containing 2.5 μg of DNA and 50 μg of Im-SPIOs; lane 7, the supernatant after adding 0.5 M KTFSA to the DNA-adsorbed Im-SPIOs. The smear band represents the released DNA after anion exchange.

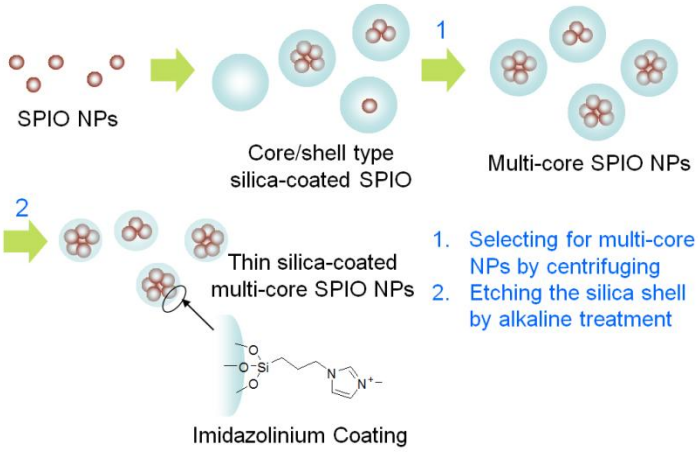

Figure 12. Schematic illustration for preparing the thin silica-coated core/shell type nanoparticles encapsulating multiple SPIO particles.

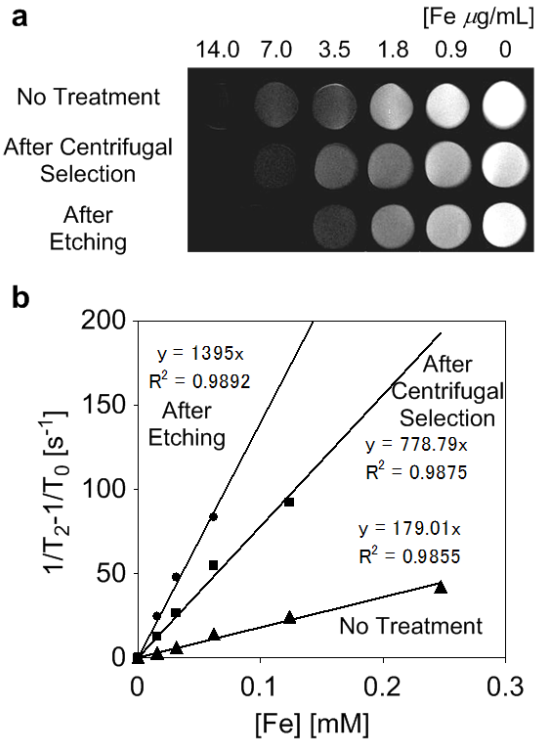

Figure 13. (a) MR imaging of various concentrations of the core/shell particles. All samples were sealed into 5 mm of glass tubes, and T_2-weighted phantom image was taken at 7 T at 25 °C. (b) T_2 dependency on weight concentration of iron of the multi-core particles after alkaline treatment (circular dots), the multi-core particles before alkaline treatment (square dots), and the sample without any treatment (triangular dots). The larger slope values represent the higher relaxation ability by the SPIOs.

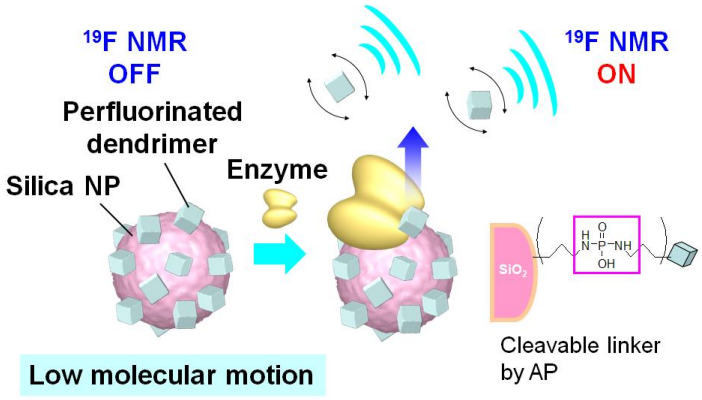

Figure 14. Regulation of ^{19}F NMR signals using silica nanoparticles as a quencher.

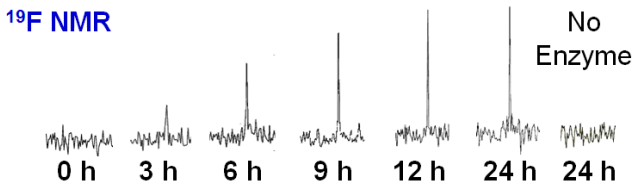

Figure 15. ^{19}F NMR spectra of fluorinated dendrimer-coated silica NPs in enzymatic hydrolysis with AP.

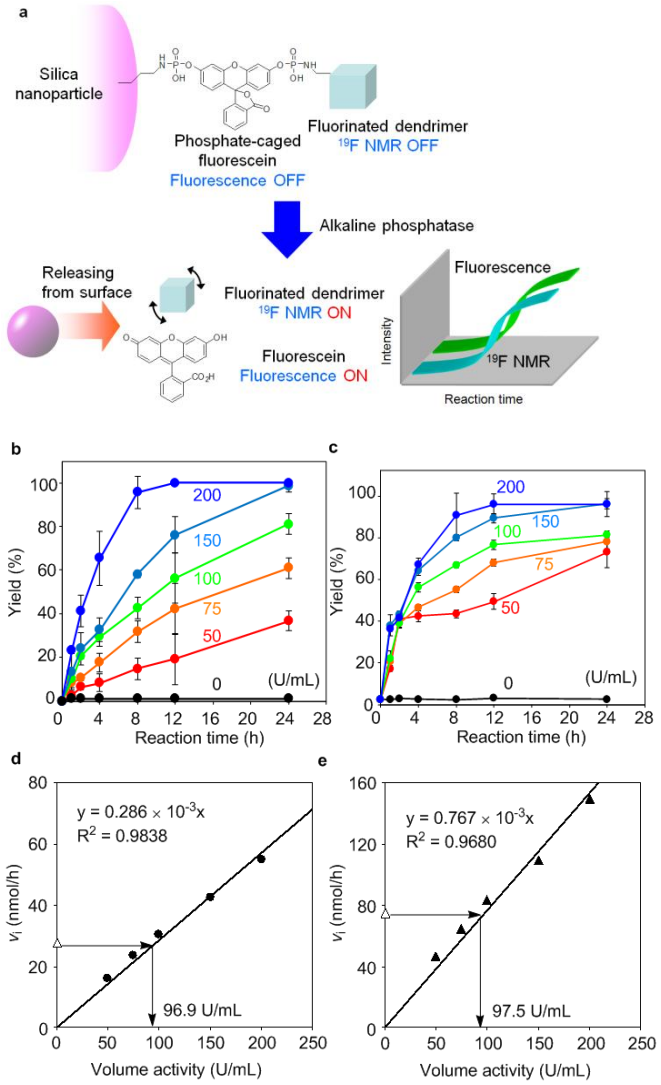

Figure 16. (a) Illustration of the bimodal probe for the quantitative assay. (b) Time-course of the intensity changes of ^{19}F NMR signals form the supernatants after enzymatic reactions. The NP probes were incubated in the reaction solutions containing various concentrations of AP. The reaction yields were monitored with ^{19}F NMR and calculated by fitting on the standards. (c) Time-courses of the emission changes at 512 nm from the 10-folds diluted supernatants after the reaction with various concentrations of AP (U/mL). (d) Fitting of the obtained value (clear triangular dot) from the ^{19}F NMR measurements to the standard line according to the results of Figure 16b. (e) Fitting of the obtained value (clear triangular dot) from the fluorescence measurements to the standard line according to the results of Figure 16c.

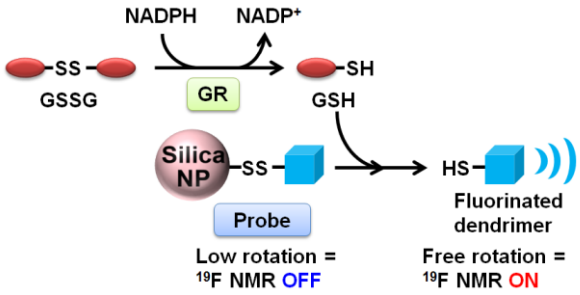

Figure 17. Schematic mechanism for GR activity using the nanoparticle-based probes.

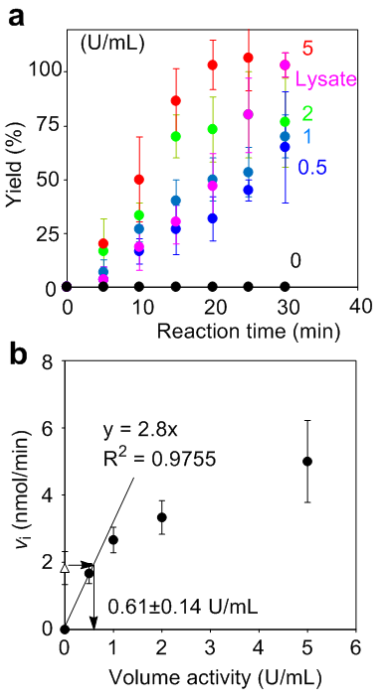

Figure 18. (a) Time-courses of the intensity changes of ^{19}F NMR signals form the supernatants after enzymatic reactions. The reaction yields were monitored with ^{19}F NMR and calculated by fitting on the standards. (b) Determination of GR activity in the HeLa cell lysate. The vertical axis represents the initial velocities (v_i) determined from the increases of the ^{19}F NMR signal intensities of the samples. Fitting of the obtained value (clear triangular dot) from the ^{19}F NMR measurements to the standard line according to the results of Figure 18a.

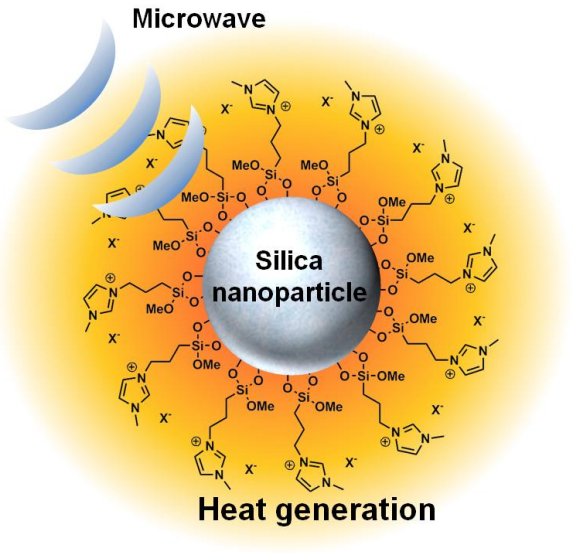

Figure 19. Illustration of the heat generation using the imidazolium-presenting silica nanoparticles.

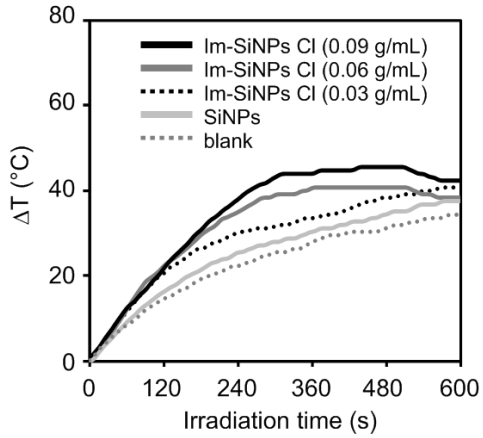

Figure 20. Temperature profiles of the samples containing silica nanoparticles and blank under microwave irradiation (50 W) for 10 min.

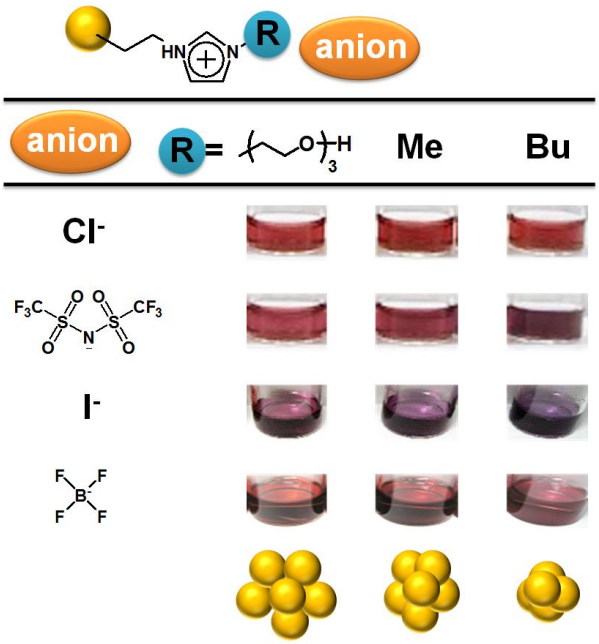

Figure 21. Chemical structures of the modified gold nanoparticles and appearances of the modified gold nanoparticles after the anion exchanges.

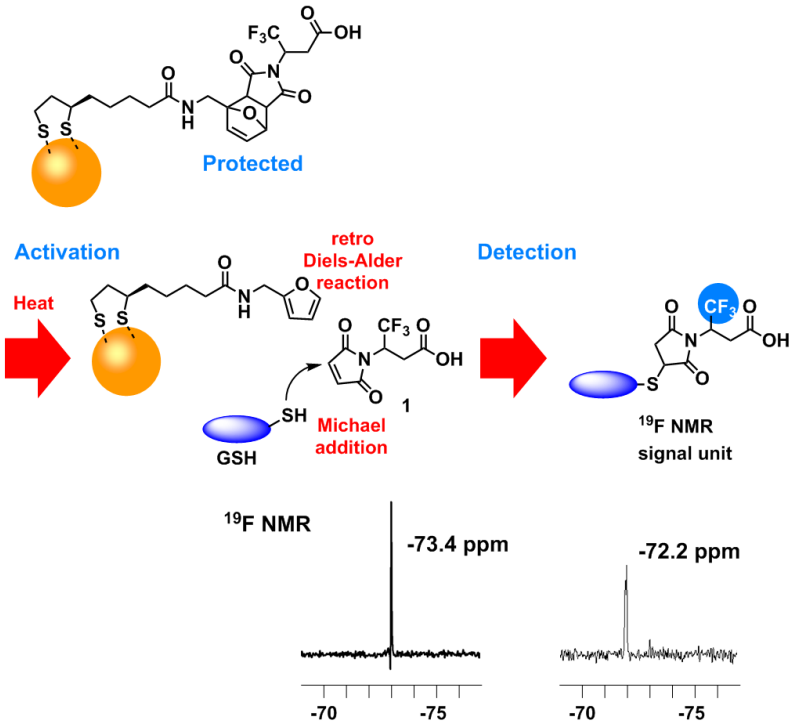

Figure 22. Structure of the linker at the surface of the nanoparticle probes and the proposed scheme of Michael addition for the GSH detection. ^{19}F NMR spectra of the signal unit were recorded before (left) and after (right) the GSH treatment.

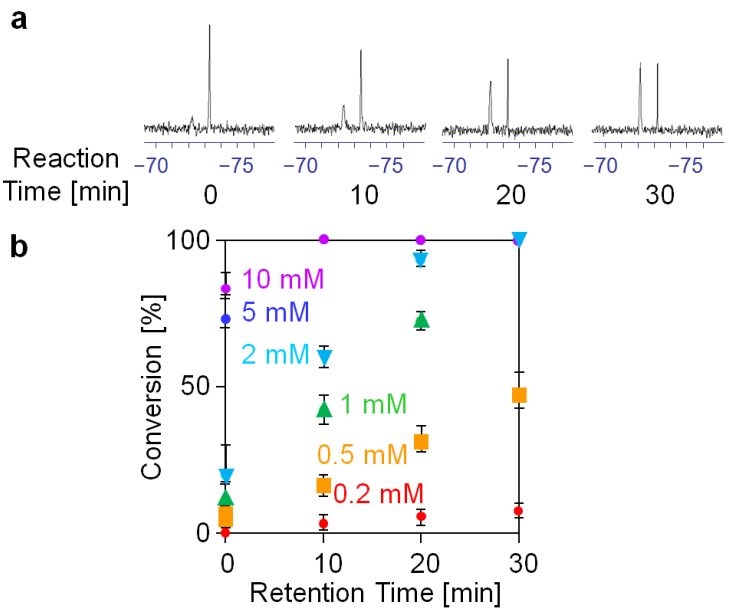

Figure 23. (a) ^{19}F NMR spectra of the mixture of nanoparticle probes and 0.5 mM of GSH after maleimide deprotection by temporary heating. (b) Time-courses of the intensity changes of ^{19}F NMR signals at –72.2 ppm with various concentrations of GSH.